Available online at website: https://journal.bcrec.id/index.php/bcrec

Bulletin of Chemical Reaction Engineering & Catalysis, 20 (4) 2025, 631-639

Original Research Article

# A Study on IIIA Group Metals (B or Ga or Tl) Doped $Mo_2C$-HZSM-5 Catalysts for Methane Dehydroaromatization

**Nagaraju Pasupulety*, Majed A Alamoudi, Abdulrahim A. Al-Zahrani**

*Chemical and Materials Engineering Department, Faculty of Engineering, King Abdulaziz University, P.O. Box 80204, Jeddah, 21589, Saudi Arabia.*

*Received: 26th August 2025; Revised: 14th September 2025; Accepted: 15th September 2025*
*Available online: 19th September 2025; Published regularly: December 2025*

## Abstract

Methane dehydroaromatization (MDA) is a promising route for direct conversion of methane into value-added aromatics such as benzene, toluene and naphthalene. This study investigates the effect of IIIA group metals like boron (B), gallium (Ga), and thallium (Tl) doped into $Mo_2C$/HZSM-5 catalysts tested for MDA at 700 °C and 1800 $mL.g_{cat}^{-1}.h^{-1}$. The influence of promoters on catalyst acidity and coke formation was investigated through various analytical techniques including $NH_3$-TPD and TPO. Among the samples, Ga-$Mo_2C$/HZSM-5 demonstrated greater benzene selectivity and consistent stability due to abundant $Mo_2C$ and low temperature coke formations. Whereas, B- or Tl-$Mo_2C$/HZSM-5 suffered from high temperature coke formations related to their greater acidity and greater extent of surface molybdenum oxidized species.



***Keywords***: MDA; Benzene; naphthalene; Mo2C; HZSM-5; Methane Dehydroaromatization

***How to Cite***: Pasupulety, N., Alamoudi, M.A., Al-Zahrani, A.A. (2025). A Study on IIIA Group Metals (B or Ga or Tl) Doped Mo2C-HZSM-5 Catalysts for Methane Dehydroaromatization. *Bulletin of Chemical Reaction Engineering & Catalysis*, 20 (4), 631-639. (DOI: 10.9767/bcrec.20477)

***Permalink/DOI***: https://doi.org/10.9767/bcrec.20477

## 1. Introduction

Methane dehydroaromatization is the direct conversion of methane into aromatic hydrocarbons such as benzene, toluene, and naphthalene, holds immense potential for chemical manufacturing [1]. Aromatic compounds are essential feedstocks in the petrochemical industry, used extensively in the production of plastics, resins, and synthetic fibre [2]. Traditionally, methane, a key natural gas component, is either used as a fuel or converted into chemicals like hydrogen or syngas through processes like steam reforming or partial oxidation. These conventional methods, however, require multiple stages, high-energy consumption, and lead to significant $CO_2$ emissions, raising sustainability concerns. Comparing with other methane reaction pathways (Fischer-Tropsch reaction, partial oxidation, oxidative coupling, $CO_2$ coupling, etc.), there is no oxygen involved in a non-oxidative MDA system which can avoid deep oxidation of methane and separation of COx from the products [3]. Furthermore, the sole reactant methane has abundant reserves [4], and the desired product benzene is an essential industrial feedstock.

Direct methane aromatization offers a more efficient route by skipping the intermediate syngas step, thereby improving overall process efficiency and potentially lowering carbon emissions. The methane aromatization reaction typically involves two key steps: the activation of methane to form reactive species and the subsequent cyclization of these intermediates to form aromatic compounds. However, methane's strong C-H bonds present a significant challenge for its activation, and thus the development of an efficient catalyst is essential for making this process practical and scalable.

Recent research has made significant strides in catalyst development, with promising results from metal-based systems, particularly those

* Corresponding Author.
Email: nsampathra@kau.edu.sa (N. Pasupulety)

utilizing molybdenum (Mo) [5-7], rhenium (Re) [8,9], and platinum (Pt) [10] as active sites. These catalysts are capable of breaking methane's robust C-H bonds and facilitating its transformation into aromatic species. However, catalyst deactivation due to coke formation and low selectivity towards the desired aromatic products continue to be major barriers to commercial viability.

Pasupulety *et al.* [11] have extensively studied the catalytic MDA process using Mo/HZSM-5 and doped M-Mo/HZSM-5 (M= Pd or Nb or Ce) catalysts to mitigate catalyst deactivation by controlling carbon deposition and optimizing reaction conditions to improve both yield and selectivity for the desired aromatic products. Among the catalysts Pd-$Mo_2C$/HZSM-5 exhibited promising benzene yield with 10 h of consistent activity. Transitions metals, such as Cu, Ni, Co, and Zn, were used as promoters aiming to alter the Fe reducibility in Fe/ZSM-5 catalysts for MDA at 750 $^oC$ [12]. Among the catalysts Cu-Fe/ZSM-5 exhibited promising benzene yield.

However, these systems still face challenges such as improving catalyst stability and minimizing by-products formations and needs novel catalyst designs for industrial feasibility. In this regard, boron (B), gallium (Ga), and thallium (Tl), promotional effect was examined for MDA process in the present work. The acid strength distribution and Brønsted/Lewis acid ratio can modified through boron doping. Further, improved dispersion of Mo particles was reported in boron modified Mo/H[B]MCM-22 catalysts [13]. Gallium can improve the molybdenum oxides reducibility and overall acidity of the catalyst there by influence the coke formations [14] in MDA reaction. Thallium in the form of hydroxide or carbonate can accelerate Suzuki-coupling reactions [15]. This study mainly focus on the improvement of the catalyst stability and selectivity towards aromatic products by employing the above properties of IIIA group metals. This is the first ever report investigated in terms of influence of IIIA group metals on active $Mo_2C$ phase formations in M-$Mo_2C$/HZSM-5 catalysts studied at 700 $^oC$ and 1800 $mL.g_{cat}^{-1}.h^{-1}$ GHSV.

## 2. Materials and Method

HZSM-5 with Si to Al ratio equals to 23 (CBV-2314), ammonium heptamolybdate tetra hydrate [$(NH_4)_6Mo_7O_{24}.4H_2O$, 99.9%], Boric acid $H_3BO_3$, gallium(III) nitrate hydrate ($Ga(NO_3)_3 \cdot xH_2O$), and thallium(III) nitrate trihydrate ($Tl(NO_3)_3.3H_2O$) was purchased from Sigma-Aldrich and used without any further purification.

### 2.1 Catalyst Synthesis

For nominal loadings of 6.0 wt.% of molybdenum, about 1.104 g of ammonium heptamolybdate tetrahydrate was dissolved in 100 ml of deionized water. In another glass beaker required quantities of other metal salts equivalent to 1.0 wt.% of metal loading were dissolved each in 50 ml of deionized water. Molybdenum and B or Ga or Tl salt solution was added simultaneously to 9.3 g of calcined HZSM-5 (Si/Al = 23) and the resultant mixture was aged for 2 h at room temperature. The excess water was evaporated by using hot plate at 120 $^oC$. The resultant solids were dried in a preheated oven at 110 $^oC$. All the dried samples were calcined at 500 $^oC$ in static air for 4 h and used in MDA process.

### 2.2. Carbidization

Carbidization transforms molybdenum oxides into molybdenum carbide, the active, stable catalyst phase that efficiently activates methane for MDA [11]. For instance, 0.5 g of calcined M-$MoO_3$/HZSM-5 (M = B or Ga or Tl) was placed in a quartz reactor under the $CH_4/H_2$ (1:4 volume ratio) gas mixture flow rate of 50 $mL.min^{-1}$. The reactor temperature was maintained at 700 $^oC$ for 20 min. Subsequently, the reactor was purged with $N_2$ gas at a flow rate of 20 $mL.min^{-1}$ for 30 min. Consequently, non-oxidative MDA reaction was carried out on these catalysts.

### 2.3. Characterizations of Catalysts

All the spent M-$Mo_2C$/HZSM-5 (M= B or Ga or Tl) catalyst samples were analyzed by using the following characterization techniques. XRD analysis was carried out on EQUINOX 1000 Inel XRD machine at Co-Kα = 1.7902 Å. BET surface area analysis was carried out on Quantachrome Nova Station (USA) at about 77 K. XPS analysis was carried out on SPECS GmbH system existing with Mg-Kα = 1253.6 eV X-ray source. Samples binding energy (BE) correction was done at C1s 284.8 eV. $NH_3$-TPD and TPO analysis experiments were carried out on Micromeritics AutoChem HP 2950 V3.02 instrument. The mass-spectral data was collected using ThermoStarTM GSD 320 quad core mass spectrometer. The m/z values monitored were: m/z= 17 ($NH_3$) or m/z = 44($CO_2$). For instance, 100 mg of spent sample was placed in a quartz reactor and pretreated at 200 $^oC$ under He gas (10 $mL.min^{-1}$) for 2 h. Then, the temperature of the sample was brought back to 40 $^oC$ and saturated with probe gas 5% $NH_3/N_2$ for 1 h. The resultant sample was purged with He (10 $mL.min^{-1}$) for 1 h. Desorption of ammonia was analyzed by TCD and mass detector in the temperature range of 40 to 800 $^oC$ at a ramping rate of 10 $^oC.min^{-1}$. Temperature programmed oxidation (TPO) experiments were carried out by using 1%$O_2$-He gas mixture with 100 mg of spent

sample. Desorption of $CO_2$ was analyzed by TCD and mass detector in the temperature range of 40-800 °C at a ramping rate of 10 °C.min$^{-1}$.

### 2.4. Catalytic Activity Tests

Catalytic activity tests were performed by using a fixed bed quartz reactor (Figure 1) with methane GHSV of 1800 mL.g$_{cat}^{-1}$.h$^{-1}$. Pre-carburized catalyst at 700 °C was introduced with $CH_4/N_2$ gas mixture at a volume ratio of 4:1. The product stream through a heated line was analyzed by a gas chromatograph (Agilent 7890 B) equipped with a HaySep D 80/100 column ($H_2$, $N_2$, CO, $CO_2$, $CH_4$, $C_2H_4$, $C_2H_6$ and $C_3H_8$) connected to TCD and a HP-1 capillary column (benzene, toluene, naphthalene and methyl naphthalene) connected to FID. The resultant spent catalysts after 15 h of reaction was denoted as $Mo_2C$/HZSM-5 and M-$Mo_2C$/HZSM-5 (M = B or Ga or Tl) for molybdenum and second metal deposited HZSM-5 catalysts respectively. The conversion of methane, product selectivity and yield was calculated according to the equations (1)-(3). The results were reproducible within the error percentage of ±0.5%. The overall carbon balance falls under 88-92% for all the studied experiments. Moles of product representing individual gas products ($CO_x$, $C_2H_4$, $C_2H_6$, and $C_3H_8$) and liquid products each such as benzene, toluene and naphthalene, etc.

$$\%\ CH_4\ Conversion = \frac{(moles\ of\ CH_{4,in} - moles\ of\ CH_{4,out})}{moles\ of\ CH_{4,in}} \times 100\% \quad (1)$$

$$\%\ Selectivity = \frac{(moles\ of\ Product_{out})}{(moles\ of\ CH_{4,in} - moles\ of\ CH_{4,out})} \times 100\% \quad (2)$$

$$\%\ Yield = \frac{(moles\ of\ Product_{out})}{(moles\ of\ CH_{4,in})} \times 100\% \quad (3)$$

## 3. Results and Discussion

### 3.1. XRD Characterization

The X-ray diffraction (XRD) patterns of all the studied spent catalysts are presented in Figure 2. Distinct diffraction peaks observed at 2θ ≈ 9.8, 10.2, 28.0, 29.0 and 29.5° correspond to HZSM-5 framework (MFI). In all the doped samples XRD patterns were observed at similar X-ray angles due to HZSM-5 confirming the structural integrity of the zeolite even after incorporation of molybdenum and various promoters (Tl, Ga, and B) [16]. In $Mo_2C$/HZSM-5 spent catalyst, X-ray patterns appeared at 2θ ≈ 32.0, 49.0 and 50.2° was assigned to $MoO_3$ phase and 2θ ≈ 30.0, 34.0 and 57.5° was ascribed to $MoO_2$ phase. Further, additional X-ray reflections at 2θ ≈ 40.0, 44.0 and 46.0° was attributed to $Mo_2C$ phase indicating partial carbidization of molybdenum oxide species under reductive carbidization conditions [11]. Among the doped catalysts, significant $Mo_2C$ phase was observed in 1Ga-$Mo_2C$/HZSM-5 catalyst with minimal molybdenum oxide signals suggesting that Ga facilitates Mo dispersion and carbidization, possibly through enhanced interaction with the zeolite surface by inhibiting Mo agglomeration [17]. Whereas, Tl and B-doped [13] catalysts exhibited weak signals for $Mo_2C$ phase indicating partial oxidation or incomplete carbidization of Mo precursors. This implies that Tl and B may stabilize molybdenum in oxide forms in the catalyst local redox environment. These results demonstrate that promoter identity plays a crucial role in tailoring the crystalline structure and phase distribution of Mo-based catalysts in MDA reaction.

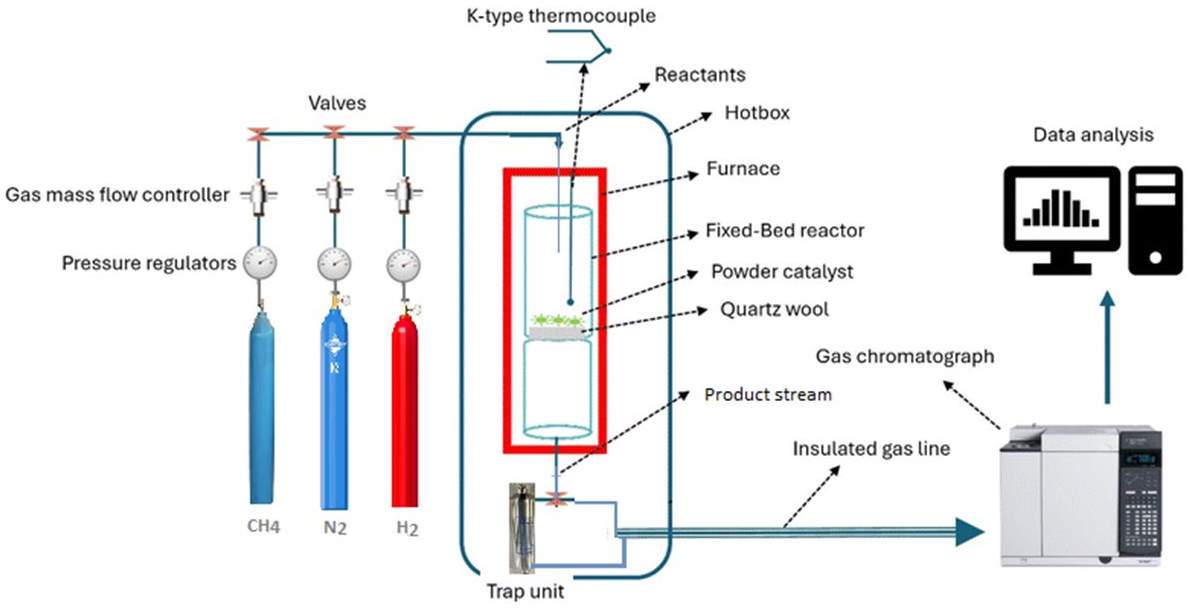


Figure 1. Schematic diagram of experimental setup.

### 3.2 $NH_3$-TPD-mass Analysis

The $NH_3$-TPD-mass profiles of spent $Mo_2C$/HZSM-5 and its doped analogues are presented in Figure 3, exhibit information about the acid strength and acidic sites distribution. All samples exhibit two main desorption regions: a low-temperature peak (~100–250 °C) attributed to weak acid sites and a broad high-temperature peak (~300–600 °C) corresponding to medium-to-strong Brønsted and Lewis acid sites [18]. The reference $Mo_2C$/HZSM-5 catalyst displayed a distinct low-temperature desorption peak centered at ~140 °C and a moderate broad peak around 365 °C for weak and strong acid sites, respectively.

Upon B and Tl modification, both peaks (low and high temperature) were widened, suggesting the enhancement of weak and medium-to-strong acid sites, likely due to their dispersion on the zeolite framework [19]. This is consistent with literature reports where B acts as a structural promoter, influencing acidity through electron withdrawal and stabilization of framework Al species [20]. On the other hand, Ga-modified sample (1Ga-$Mo_2C$/HZSM-5) exhibit distinctly different behavior. The Ga-promoted catalyst shows suppressed low-temperature desorption and a broad weak signal at ~400 °C, indicating reduction in both weak and strong acid sites, possibly due to Ga occupying or neutralizing acidic sites [21] of HZSM-5. Overall, the $NH_3$-TPD-mass analysis reveals that Tl and B doping enhanced the total acidity and acid strength, while Ga reduce acid site density and/or strength, thus significantly influencing the potential catalytic behavior in MDA reaction.

### 3.3 XPS Analysis

Mo 3d XPS spectra of spent $Mo_2C$/HZSM-5 and its doped variants (1B-$Mo_2C$, 1Ga-$Mo_2C$, and 1Ti-$Mo_2C$) reveal distinct surface species in Figure 4a corresponds to different molybdenum oxidation states. Peaks at higher binding energies, in the range of 231.8–232.2 eV, correspond to $Mo^{6+}$, indicative of $MoO_3$ or other oxidized Mo surface species [22,23]. Deconvoluted peaks at binding energies around 230.5-231.2 eV are attributed to the components of $Mo^{4+}$, commonly assigned to $MoO_2$-like species [24]. Binding energy peaks, close to 227.0-228.0 eV, are assigned to carbidic Mo species (Mo-C bonds), characteristic of $Mo_2C$ [25]. The relative abundance of these species varies with the type of dopant introduced. For instance, boron and thallium incorporation leads to increased $Mo^{6+}$ content, suggesting enhanced surface oxidation, whereas gallium doping stabilizes a greater proportion of $Mo^{4+}$ and Mo-C, possibly favoring higher catalytic activity due to preserved metallic or carbidic character. These findings demonstrate that dopants modulate the electronic structure and surface chemistry of Mo species, which in line with XRD data.

The XPS spectra presented in Figure 4b correspond to B 1s, Ga 2p, and Tl 4f regions, confirming the presence and oxidation states of the respective dopants in the $Mo_2C$/HZSM-5 catalyst systems. The B 1s spectrum (top left) displays a peak centered at 193.2 eV, characteristic of boron in oxidized form ($B^{3+}$), typically assigned to $BO_3$ or tetrahedral boron in a silicate framework in zeolite structures [26]. The Ga 2p peak (top right), appearing near 1118.1 eV, corresponds to $Ga^{3+}$, indicating $Ga_2O_3$ or incorporated into the zeolite lattice as isolated $Ga^{3+}$ sites, which are known to influence acid properties and catalytic activity [27,28]. The Tl 4f

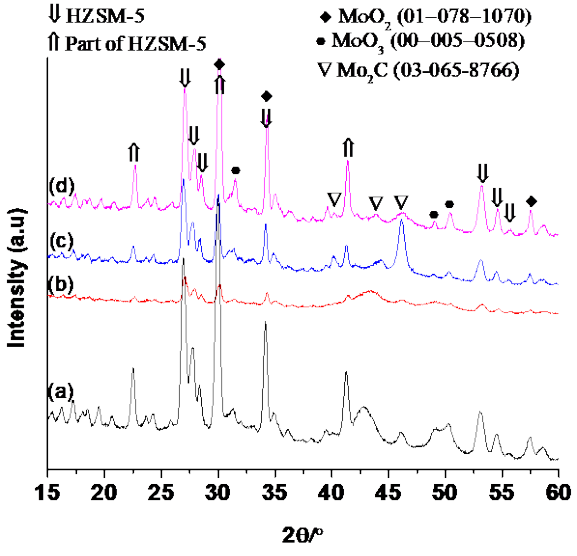


Figure 2. XRD spectra of spent catalysts (a) $Mo_2C$/HZSM-5 (b) 1B-$Mo_2C$/HZSM-5 (c) 1Ga-$Mo_2C$/HZSM-5 (d) 1Tl- $Mo_2C$/HZSM-5.

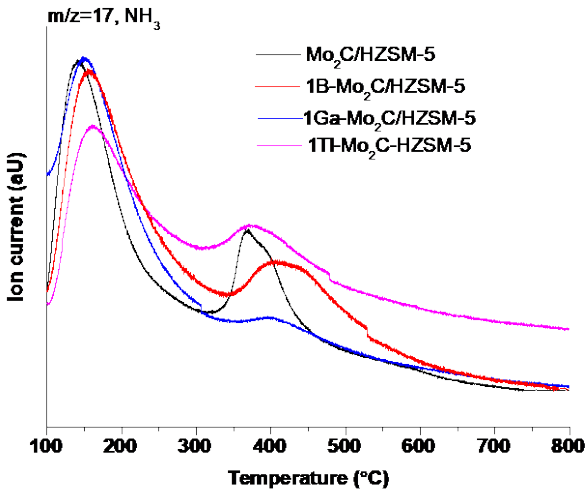


Figure 3. $NH_3$-TPD-mass analysis of spent catalysts.

spectrum (bottom) shows well-resolved spin-orbit doublets with peaks centered at 118.2 eV (Tl $4f_{7/2}$) and 122.8 eV (Tl $4f_{5/2}$), consistent with $Tl^+$ species, commonly observed in thallium-exchanged zeolites or $Tl_2O$ [29]. Minor features overlapping near 119.0 eV are likely due to the Al 2s signal from the HZSM-5 framework [30]. These spectra confirm successful incorporation of B, Ga, and Tl into $Mo_2C$/HZSM-5 with surface concentration of 0.21%, 0.09% and 0.12%, respectively.

### 3.4. TPO-Mass Analysis

The $CO_2$ evolution profiles (m/z = 44) as a function of temperature provide insights into the coke oxidation behavior of spent $Mo_2C$/HZSM-5

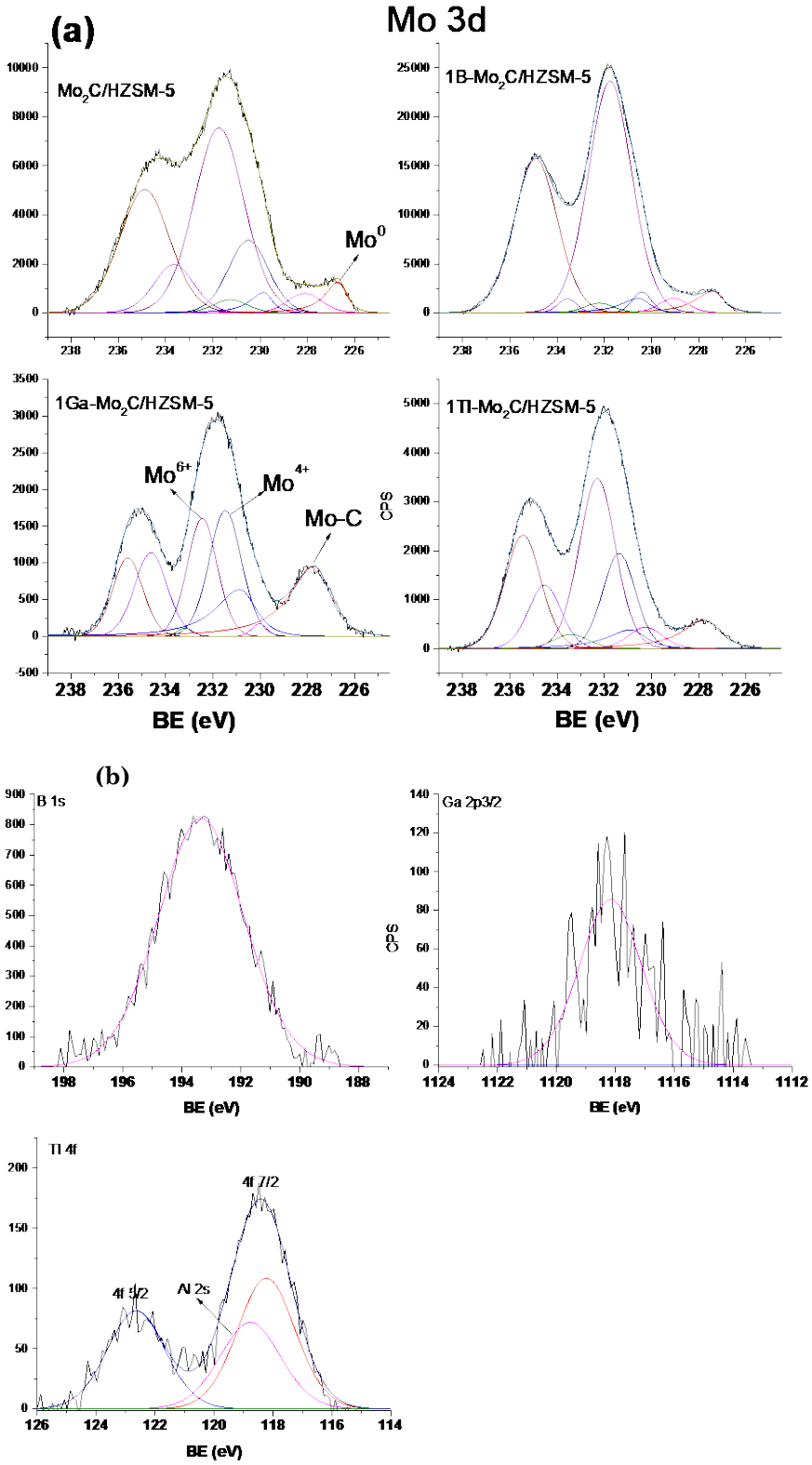


Figure 4. (a). XPS analysis of Mo 3d orbital of spent catalysts; (b). XPS analysis of spent B or Ga or Tl dopants.

catalyst and their doped variants in Figure 5. The undoped $Mo_2C$/HZSM-5 shows a $CO_2$ peak centered at approximately 465 °C, indicating the surface carbon species (coke) were oxidized or removed. However, with the addition of dopants, distinct changes were observed. The 1Tl- and 1B-$Mo_2C$/HZSM-5 sample exhibits $CO_2$ evolution peak ~445 °C, suggesting the formation of more reactive, easily oxidizable coke species [31]. On the other hand, 1Ga-$Mo_2C$/HZSM-5 sample exhibited $CO_2$ desorption peak at 425 °C, implying modification of coke nature and quantity. The lower $CO_2$ evolution for Ga-modified catalysts may indicate altered acid site distribution, which affects the deactivation behavior [32,33]. Furthermore, unmodified and Tl-doped catalysts showed small portion of high temperature (~600 °C) $CO_2$ desorptions suggest stable coke formations. Overall, strong acidity existed in unmodified, B- and Tl-doped catalysts produced stable coke formations, which led to catalyst deactivation in MDA process.

### 3.5 BET Surface Area and Pore Size Distribution Data

The BET surface and pore volume data of spent catalysts presented in Table 1. It is obvious that bare support displayed highest BET surface area and pore volume. However, Mo loaded spent MDA catalyst possessed a great decrease in the BET surface area and pore volume associated with pore blockage by coke. On the other side, B-, Ga- and Tl-doping with Mo decreased the surface area and pore volume further suggesting that dopants are existed in the HZSM-5 pores. Similar results were observed by Pasupulety *et al.* [11] and Perez-Lopez *et al.* [12] for metal doped Mo/HZSM-5 and Fe/ZSM-5 catalysts.

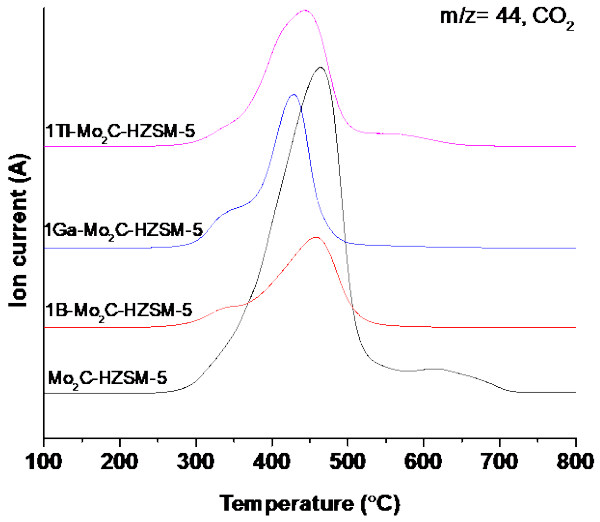


Figure 5. TPO-mass analysis of spent catalysts.

### 3.6 Catalytic Activity Results

The $CH_4$ conversion data illustrates the influence of dopants on the catalytic performance of M-$Mo_2C$/HZSM-5 catalysts in Figure 6a at 700 °C. Among the samples, B-$Mo_2C$/HZSM-5 exhibited the highest methane conversion (~22.0%), followed by the undoped $Mo_2C$/HZSM-5 (~16.0%), Tl-$Mo_2C$/HZSM-5 (~15.0%) and Ga-$Mo_2C$/HZSM-5 (~13.0%). This trend suggests that boron incorporation enhanced methane activation, potentially by increased Brønsted acidity and there by improved oligomerization of xHC-CHx products on the catalyst [34,35]. Ga-modification lead to lowest performance due to balance between overall acidity and $Mo_2C$ phase. These results indicate that dopant selection played a critical role in tailoring the catalyst surface acidic properties for methane conversion.

The selectivity plot in Figure 6b reveals the significant role of dopants in steering product distribution during MDA on $Mo_2C$/HZSM-5 catalysts. B-$Mo_2C$/HZSM-5 exhibits the highest naphthalene selectivity (~47.0%) and the lowest benzene selectivity (~32.5%), suggesting that boron promotes aromatic ring growth or secondary aromatization reactions, potentially due to enhanced Brønsted acidity and increased coke formation pathways [36]. In contrast, Ga-modified catalysts show a marked increase in benzene selectivity, reaching ~66.0%, while naphthalene selectivity drops below 20.0%. The results indicate that Ga suppress excessive condensation reactions, favoring single-ring aromatic products [37,38]. While, Tl-doping achieving moderate selectivity for benzene and naphthalene due to its suitable acid strength and metal-support interactions. For all the studied

Table 1. BET surface area and pore volume data of spent catalysts.

| Sample | BET-SA ($m^2.g^{-1}$) | Pore volume ($cm^3.g^{-1}$) | | $NH_3$-TPD ($\mu mol.g^{-1}$) | |
|---|---|---|---|---|---|
| | | Micro | Meso | weak | strong |
| HZSM-5 | 318.0 | 0.174 | 0.010 | 740 | 380 |
| $Mo_2C$/HZSM-5 | 234.0 | 0.132 | 0.009 | 536 | 320 |
| B-$Mo_2C$/HZSM-5 | 218.0 | 0.131 | 0.008 | 580 | 330 |
| Ga-$Mo_2C$/HZSM-5 | 209.0 | 0.129 | 0.007 | 480 | 50 |
| Tl-Mo2C/HZSM-5 | 215.0 | 0.131 | 0.009 | 520 | 200 |

catalysts, linear hydrocarbons and toluene formations were found less than 6.0%. These findings suggest that dopants not only affect methane activation and coke resistance but also control hydrocarbon transformation pathways with product specificity.

### 3.7. Time on Stream Studies

The time-on-stream data (Figure 7) further elucidated the role of dopants in governing catalyst deactivation during MDA process. The Ga-$Mo_2C$/HZSM-5 catalyst demonstrated the most stable performance, maintained a benzene yield of ~8.5% with only a slight decline over 15 h. This excellent stability aligns with XPS results showing $Ga^{3+}$ incorporation resulted in modified Brønsted acidity suppressed polyaromatic growth [39]. Consistently, TPO analysis showed low temperature $CO_2$ release, indicating controlled coke formation in this catalyst. In contrast, B-$Mo_2C$/HZSM-5 despite its initial comparable benzene yields, it exhibited the most severe deactivation and dropped benzene yield to 5.25% after 15 hrs. It was likely due to strong coking tendency on B, which gradually blocks MDA active sites [40]. The un-doped $Mo_2C$/HZSM-5 and Tl-doped catalysts showed moderate stability, suffers from gradual deactivation, consistent with their higher naphthalene selectivity and coke accumulation observed in their TPO profile. Overall, the results indicates Ga-doping optimized the balance between activity, selectivity, and stability, making it the most promising modification for sustained MDA performance.

## 4. Conclusions

This study demonstrates that Group IIIA metal doping significantly alters the physicochemical properties and catalytic behaviour of reference $Mo_2C$/HZSM-5 catalyst in MDA process at 700 °C. Among the catalysts, Ga-doping in $Mo_2C$/HZSM-5 emerged as the most promising strategy resulted in greater benzene selectivity (66.0%) with 15 h of consistent activity due to abundant $Mo_2C$ phase and with appropriate acidity. However, boron addition enhanced the methane conversion (22.0%), further, promotes naphthalene and high temperature coke formations through its greater acidity. Whereas, Tl-doping eventually yielded moderate methane conversion and benzene selectivity further, gradually deactivated after 7hrs was associated with weak active site efficiency. These findings provide a valuable foundation for rational design of MDA catalysts.

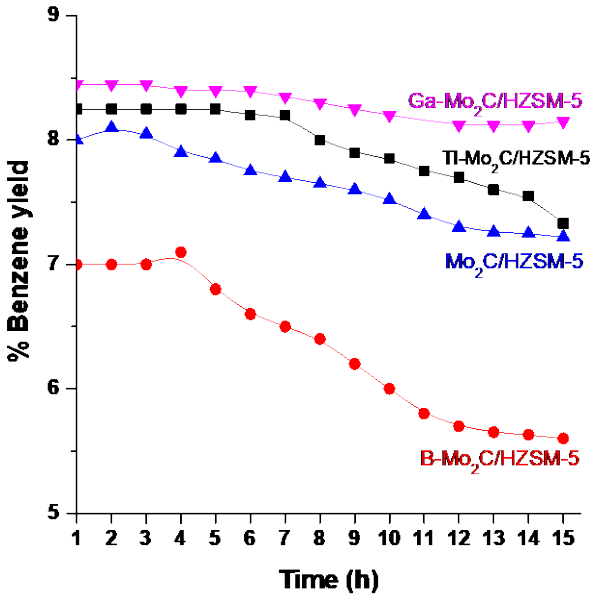


Figure 7. Time on stream studies at 700 °C and 1800 mL.$g_{cat}^{-1}$.$h^{-1}$.

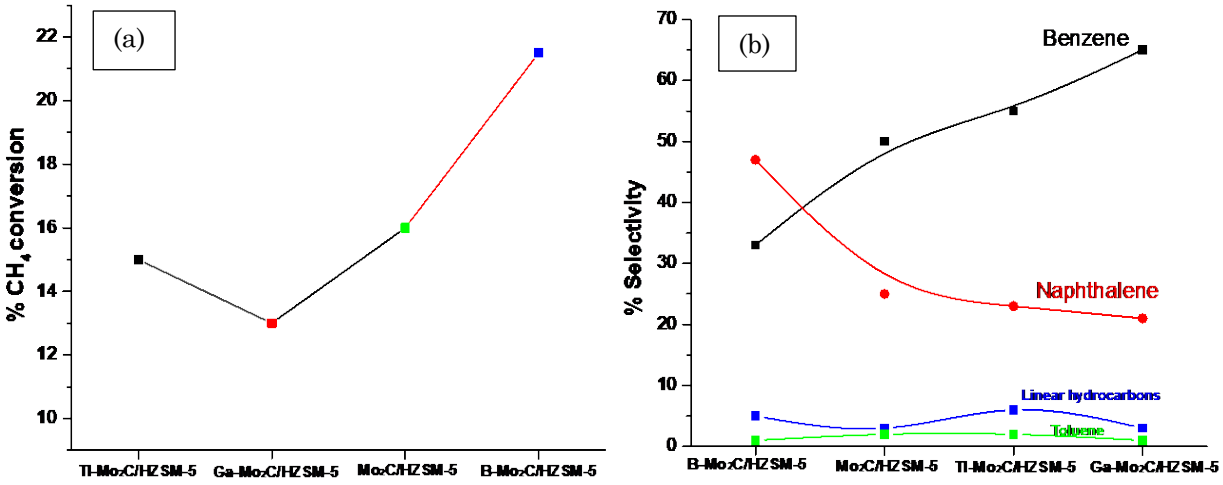


Figure 6. (a) MDA activity at 700 °C and 1800 mL.$g^{-1}$.$h^{-1}$ GHSV; (b) MDA selectivity.

**Acknowledgments**

This Project was funded by Deanship of Scientific Research (DSR) at King Abdulaziz University, Jeddah, under the Grant no.G: 355-135-1443. The authors, therefore, acknowledge with thanks DSR for technical and financial support.

**CRedit Author Statement**

Author Contributions: N. Pasupulety: Conceptualization, Methodology, Investigation, Resources, Data Curation, Writing, Review and Editing, Supervision; M. A. Alamoudi: Formal Analysis, Data Curation, Visualization, Project Administration; A. A. Zahrani: Validation, Review and Editing. All authors have read and agreed to the published version of the manuscript.

**References**

[1] Zhu, P., Bian, W., Liu, B., Hao, D., Lucun, W., Xiaozhou, H., Stephanie, L.S., Feng, L., Chuancheng, D., Dong, D., Pei, D., Hanping, D (2024). Direct conversion of methane to aromatics and hydrogen via a heterogeneous trimetallic synergistic catalyst. *Nature Communications*. 15, 3280. DOI: 10.1038/s41467-024-47595-9.

[2] Hu, J., Yang, C., Liu, B., Zhao, X., Wang, Y., Wang, X., Liu, J., Guan, J. (2023). Improving the methane aromatization activity and anti-carbon deposition on MCM-22 through nano α-$MoO_3$ modification. *New Journal of Chemistry*. 47, 2949–2956. DOI: 10.1039/D2NJ05415A.

[3] Spivey, J.J., Hutchings, G. (2014). Catalytic aromatization of methane. *Chemical Society Reviews*. 43, 792–803. DOI: 10.1039/C3CS60259A.

[4] Emmanuel, A., Devi, P.R., Mathew, T.V. (2024). Reserves and natural gas sources of methane emissions: Greenhouse gas. In *Greenhouse Gases Emissions and Climate Change*, 53–70. DOI: 10.1016/B978-0-443-19231-9.00017-X.

[5] Liu, Y., Ćoza, M., Drozhzhin, V., van den Bosch, Y., Meng, L., van de Poll, R., Hensen, E.J.M., Kosinov, N. (2023). Transition-metal catalysts for methane dehydroaromatization (Mo, Re, Fe): Activity, stability, active sites, and carbon deposits. *ACS Catalysis*. 13(1), 1–10. DOI: 10.1021/acscatal.2c04962.

[6] Kosinov, N., Coumans, F.J.A.G., Uslamin, E.A., Wijpkema, A.S.G., Mezari, B., Hensen, E.J.M. (2017). Methane dehydroaromatization by Mo/HZSM-5: Mono- or bifunctional catalysis. *ACS Catalysis*. 7(1), 520–529. DOI: 10.1021/acscatal.6b02497.

[7] Qi, S., Yang, B. (2004). Methane aromatization using Mo-based catalysts prepared by microwave heating. *Catalysis Today*. 98, 639–645. DOI: 10.1016/j.cattod.2004.09.049.

[8] López-Martín, A., Sini, M.F., Cutrufello, M.G., Caballero, A., Colón, G. (2022). Characterization of Re-Mo/ZSM-5 catalysts: How Re improves the performance of Mo in the methane dehydroaromatization reaction. *Applied Catalysis B: Environmental*. 304, 120960. DOI: 10.1016/j.apcatb.2021.120960.

[9] Wang, L., Ohnishi, R., Ichikawa, M. (2000). Selective dehydroaromatization of methane toward benzene on Re/HZSM-5 catalysts and effects of $CO/CO_2$ addition. *Journal of Catalysis*. 190(2), 276–283. DOI: 10.1006/jcat.1999.2748.

[10] Tshabalala, T.E., Coville, N.J., Anderson, J.A., Michael, S.S. (2021). Dehydroaromatization of methane over noble metal loaded Mo/H-ZSM-5 zeolite catalysts. *Applied Petrochemical Research*. 11, 235–248. DOI: 10.1007/s13203-021-00274-y.

[11] Pasupulety, N., Al-Zahrani, A.A., Daous, M.A., Driss, H., Petrov, L.A. (2021). Methane aromatization study on M-$Mo_2C$/HZSM-5 (M = Ce or Pd or Nb) nanomaterials. *Journal of Materials Research and Technology*. 14, 363–373. DOI: 10.1016/j.jmrt.2021.06.058.

[12] Denardin, F., Perez-Lopez, O.W. (2019). Tuning the acidity and reducibility of Fe/ZSM-5 catalysts for methane dehydroaromatization. *Fuel*. 236, 1293–1300. DOI: 10.1016/j.fuel.2018.09.128.

[13] Gan, Y., Xu, Y., Zhang, P., Wang, W., Liu, W., Li, R., Xu, X., Wu, L., Tang, Y., Tan, L. (2024). Boron doped Mo/HMCM-22 catalyst for improving coke resistance in methane dehydroaromatization. *Chemical Engineering Science*. 299, 120485. DOI: 10.1016/j.ces.2024.120485.

[14] Dutta, K., Li, L., Gupta, P., Pacheco Gutierrez, D., Kopyscinski, J. (2018). Direct non-oxidative methane aromatization over gallium nitride catalyst in a continuous flow reactor. *Catalysis Communications*. 106, 16–19. DOI: 10.1016/j.catcom.2017.12.005.

[15] Carneiro, V.M.T., Longo, L.S., Silva, L.F. (2015). Sustainable catalysis using non-endangered metals. In North, M. (Ed.), *Sustainable Catalysis: With Non-endangered Metals*, Part 2, 212–230. The Royal Society of Chemistry: Cambridge

[16] Rahele, M., Lars-Åke, N., Joseph, H., Jun, L., Michel, W.B., Johanna, R. (2015). Synthesis of two-dimensional molybdenum carbide, $Mo_2C$, from the gallium based atomic laminate $Mo_2Ga_2C$. *Scripta Materialia*. 108, 147–150. DOI: 10.1016/j.scriptamat.2015.07.003.

[17] Matthew, Y., Peng, H., Jack, J., Shijun, M., Aiguo, W., Shiyu, K., Richard, G., Lijia, L,, Hua, S. (2018). Co-aromatization of methane with olefins: The role of inner pore and external surface catalytic sites. *Applied Catalysis B: Environmental*. 234, 1–10. DOI: 10.1016/j.apcatb.2018.04.034.

[18] Busca, G. (2017). Acidity and basicity of zeolites: A fundamental approach. *Microporous and Mesoporous Materials*. 254, 3–16. DOI: 10.1016/j.micromeso.2017.04.007.

[19] Medak, G., Puškarić, A., Bronić, J. (2023). The Influence of Inserted Metal Ions on Acid Strength of OH Groups in Faujasite. *Crystals*. 13(2), 332. DOI: 10.3390/cryst13020332.

[20] Chen, J., Liang, T., Li, J., Wang, S., Qin, Z., Wang, P., Huang, L., Fan, W., Wang, J. (2016). Regulation of Framework Aluminum Siting and Acid Distribution in H-MCM-22 by Boron Incorporation and Its Effect on the Catalytic Performance in Methanol to Hydrocarbons. *ACS Catalysis*. 6(4), 2299–2313. DOI: 10.1021/acscatal.5b02862.

[21] Mudi, X., Enhui, X., Xiuzhi, G., Yongrui, W., Ying, O., Guangtong, X., Yibin, L., Xingtian, S. (2019). Ga Substitution during Modification of ZSM-5 and Its Influences on Catalytic Aromatization Performance. *Ind. Eng. Chem. Res*. 58 (17), 6970–6981. DOI: 10.1021/acs.iecr.9b00295.

[22] Khademi, A., Azimirad, R., Zavarian, A., Moshfegh, A. (2009). Growth and Field Emission Study of Molybdenum Oxide Nanostars. *Journal of Physical Chemistry C*. 113(45), 19298–19304. DOI: 10.1021/jp9056237.

[23] Hu, H., Wachs, I.E., Bare, S.R. (1995). Surface Structures of Supported Molybdenum Oxide Catalysts: Characterization by Raman and Mo L3-Edge XANES. *The Journal of Physical Chemistry*. 99(27), 10897–10910. DOI: 10.1021/j100027a030.

[24] Briggs, D., Seah, M.P. (1990). Practical Surface Analysis, 2nd ed. Wiley: Chichester, UK.

[25] Pasupulety, N., Al-Zahrani, A.A., Daous, M.A., Driss, H., Petrov, L.A. (2020). Studies on molybdenum carbide supported HZSM-5 (Si/Al = 23, 30, 50 and 80) catalysts for aromatization of methane. *Arabian Journal of Chemistry*. 13(5), 5199–5207. DOI: 10.1016/j.arabjc.2020.02.016.

[26] Li, H., Zhang, W., Liu, Y. (2020). HZSM-5 zeolite supported boron-doped TiO2 for photocatalytic degradation of ofloxacin. *Journal of Materials Research and Technology*. 9(3), 2557–2567. DOI: 10.1016/j.jmrt.2019.12.086.

[27] Uslamin, E.A., Luna-Murillo, B., Kosinov, N., Bruijnincx, P.C.A., Pidko, E.A., Weckhuysen, B.M., Hensen, E.J.M. (2019). Gallium-promoted HZSM-5 zeolites as efficient catalysts for the aromatization of biomass-derived furans. *Chemical Engineering Science*, 198, 305–316. DOI: 10.1016/j.ces.2018.09.023.

[28] Xin, M., Xing, E., Gao, X., Wang, Y., Ouyang, Y., Xu, G., Luo, Y., Shu, X. (2019). Ga substitution during modification of ZSM-5 and its influences on catalytic aromatization performance. *Industrial & Engineering Chemistry Research*, 58(17), 6970–6981. DOI: 10.1021/acs.iecr.9b00295.

[29] Gaur, G.K., Srivastava, S. (2012). Characterization, XPS and toxicological study of organothallium (III) compounds with Schiff base ligands. *Crystal Structure Theory and Applications,* 1(3), 97–99. DOI: 10.4236/csta.2012.13018.

[30] Leclair, P., Kohlhepp, J.T., Smits, A.A., Swagten, H.J.M. (2000). Optical and in situ characterization of plasma oxidized Al for magnetic tunnel junctions. *Journal of Applied Physics*, 87(9), 6070–6072. DOI: 10.1063/1.372615.

[31] Huang, X., Wang, L., Gao, L., Jiao, X., Guo, X. (2025). Boron assists molybdenum to be confining single atoms for methane dehydroaromatization. *Fuel*, 384, 134040. DOI: 10.1016/j.fuel.2024.134040.

[32] Guisnet, M., Gilson, J.-P. (2002). Zeolites for Cleaner Technologies. Imperial College Press: London, UK.

[33] Song, C., Gim, M. Y., Lim, Y. H., & Kim, D. H. (2019). Enhanced yield of benzene, toluene, and xylene from the co-aromatization of methane and propane over gallium supported on mesoporous ZSM-5 and ZSM-11. *Fuel*, 251, 404–412. DOI: 10.1016/j.fuel.2019.04.079.

[34] Sonit, B., Ali, H. M., Tuhin, S.K., Pant, K.K. (2020). Boric acid treated HZSM-5 for improved catalyst activity in non-oxidative methane dehydroaromatization. *Catal. Sci. Technol.* 10, 3857-3867. DOI: 10.1039/D0CY00286K.

[35] Huang, M., Li, J., Liu, Q., Zhang, M., Liu, Z., Gao, B. (2023). Enhanced catalytic performance of the hollow Mo/HZSM-5 nanocrystal for methane dehydroaromatization. *Fuel*, 334 (Part 2), 126765. DOI: 10.1016/j.fuel.2022.126765.

[36] Liu, S., Wang, L., Ohnishi, R., Ichikawa, M. (1999). Bifunctional catalysis of Mo/HZSM-5 in the dehydroaromatization of methane to benzene and naphthalene: XAFS/TG/DTA/MASS/FTIR characterization and supporting effects. *Journal of Catalysis*, 181, 175–188. DOI: 10.1006/jcat.1998.2310.

[37] Lee, B.J., Hur, Y.G., Kim, D.H., Lee, S.H., Lee, K.-Y. (2019). Non-oxidative aromatization and ethylene formation over Ga/HZSM-5 catalysts using a mixed feed of methane and ethane. *Fuel*, 253, 449–459. DOI: 10.1016/j.fuel.2019.05.014.

[38] Mishra, D., Modak, A., Pant, K.K., Zhao, G.X.S. (2022). Improved benzene selectivity for methane dehydroaromatization via modifying the zeolitic pores by dual-templating approach. *SSRN Electronic Journal*. DOI: 10.2139/ssrn.4121584.

[39] Ertl, G., Knözinger, H., Schüth, F., Weitkamp, J. (2008). Handbook of Heterogeneous Catalysis. Wiley-VCH: Weinheim, Germany

[40] Deepti, M., Arindam, M., Pant, K.K., Xiu, S. Z. (2022). Improved benzene selectivity for methane dehydroaromatization via modifying the zeolitic pores by dual-templating approach. *Microporous and Mesoporous Materials*. 344, 112172. DOI: 10.1016/j.micromeso.2022.112172.